# SEISMIC SSSI ANALYSIS FOR DEEPLY EMBEDDED SMR STRUCTURE FOUNDED DIFFERENT NONUNIFORM SOIL SITE CONDITIONS

**Dan M Ghiocel[1] and Luben Todorovski [2]**

[1] President, GP Technologies, Inc., New York, USA (dan.ghiocel@ghiocel-tech.com)
[2] Principal Engineer, GE Hitachi, Wilmington (luben.todorovski@ge.com)

## ABSTRACT

The paper investigates the effects of the structure-soil-structure interaction (SSSI) for a typical deeply embedded SMR structure subjected to coherent and incoherent ground motions. The SSSI model includes a deeply embedment SMR structure and a large-size neigboring Auxiliary Building (AB) structure with a shallow embedment. Two nonuniform soil site conditions are considered including a deep soft soil deposit and a shallow stiff soil layer above bedrock. The seismic input motion is defined by both a coherent input and an incoherent input. Incoherent motion is defined based on the Abrahamson coherence functions (Abrahamson, 2007). The variation of the coherence function with depth is also included per the US NRC DSRS SRP 3.7.2 requirements for embededd SMRs. The seismic SSI analysis results indicated significant SSSI effects for both sites on the SMR and AB structure responses. Computed ISRS in SMR and AB are compared for the standalone SSI and the SSSI analysis cases. The tendency is that when the SMR SSSI response increases, then, the AB SSSI response decreases, or vice-versa. Noticeably, the SSSI effects on SMR are much larger for the shallow soil layer site than the deep soil site. The effects of motion incoherency are important for seismic forces and moments in the SMR embedded walls. The motion incoherency variation with depth could be significant on the computed ISRS in SMR, as shown herein for the shallow soil layer site.

## BRIEF DESCRIPTION OF SSSI MODEL AND SELECTED SITE CONDITIONS

Two specific site conditions were considered (Todorovski et al., 2022): 1) Site 1, a deep soft soil deposit, close to the 270-60 soil profile, and 2) Site 2, a shallow firm soil layer above a hardrock formation, close to the 500-21 soil profile. The seismic input frequency content corresponded to two site-specific surface GRS for the two site conditions. The maximum ground acceleration was assumed to be 0.30g. Figure 1 describes the two site-specific soil layering and seismic GRS inputs for the SSI analyses. The coherent and incoherent SSSI calculations are performed using the ACS SASS I software (GP Technologies, 2023).

Figure 2 shows the seismic SSSI model including the SMR and AB embedded structures. The SMR structure is a reinforced concrete (RC) shearwall structure with a horizontal section size of 100ft by 100ft, and a total vertical size of 162.50 ft with an embedment of 118 ft and a super-structure height above ground of 44.50 ft. The AB structure has a horizontal size of 196 ft x 80 ft and an embedment of 21.4 ft. The large AB structure weight is about two-thirds of the SMR weight. The SMR excavation model includes 30 embedment soil layers. It should be noted that for Site 2, the SMR foundation depth of 118 ft is inside the hard-rock formation that is between 80 ft and 330 ft depth having an average Vs of about 6,500 fps.

The seismic incoherent SSSI analysis is performed based on the Abrahamson coherence functions for the soil sites and the rock sites, respectively (Abrahamson, 2007). The variation of the motion incoherency with depth is also included by using multiple coherence functions variable with depth. It should be noted that the coherence function decay with frequency is much faster at the ground surface than at the SMR foundation level per the 2007 EPRI TR 1015110 guidance and the US NRC DSRS SRP 3.7.2 requirements for deeply embedded SMRs. Based on Abrahamson's recommendation mentioned in the same 2007 EPRI report, the coherence function was defined varying from the Abrahamson coherence function for soil sites at the ground surface to the Abrahamson coherence for hard-rock sites at the SMR foundation

level as shown in Figure 3. The lowest-value coherence functions in Figure 3 correspond to the ground surface level.

The two coherence functions at the surface and SMR foundation levels, for both horizonal and vertical directions, are plotted in Figure 4. The same line colour was used for the two-level coherence functions computed for the same relative distance. The lower coherence amplitude curves correspond to the surface level for which the incoherency is higher, having a faster amplitude decay with frequency.

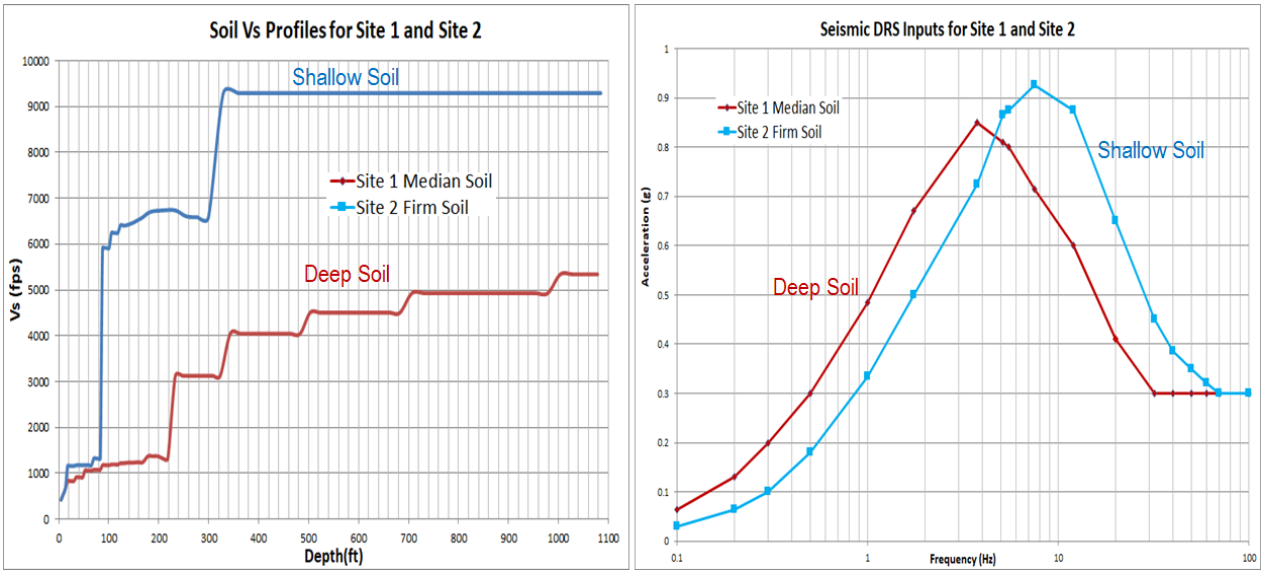


Figure 1. The Vs Soil Profiles (left) and Input GRS at Ground Surface (right) for Site 1 and Site 2

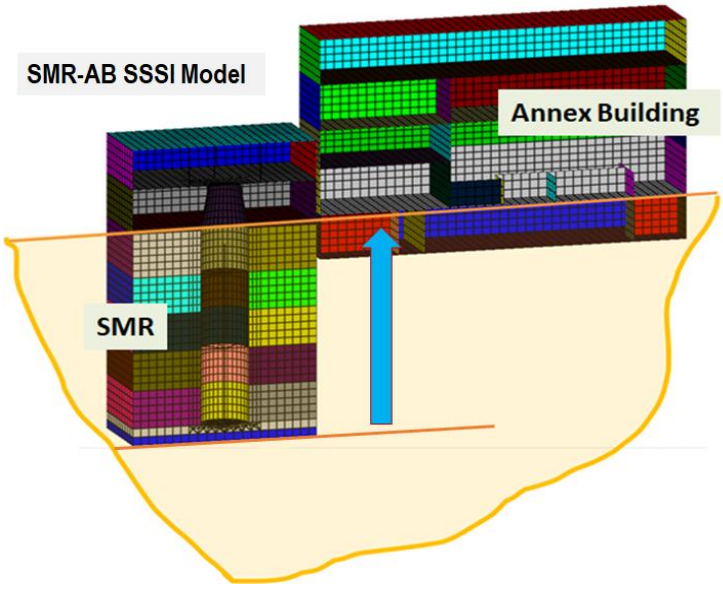


Figure 2. Deeply Embedded SMR-AB SSSI Model

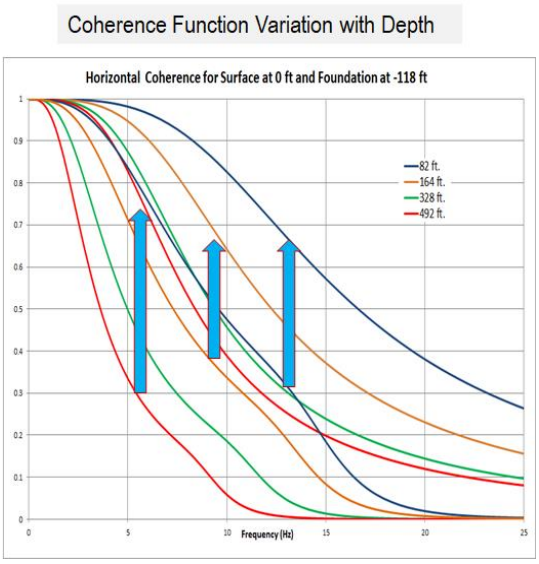


Figure 3. Coherence Variation with Depth

For the deeply embedded SMR-AB SSSI modeling, the ACS SASSI Fast Flexible Volume (FFV) approach was considered. The FFV approach which is a special case of the Extended Subtraction Method (ESM) recommended in ASCE 4-16. The FFV interaction nodes included all the excavation outer surface nodes plus additional 11 interaction node internal layers for the SMR excavation and 3 internal node layers for the AB excavation. The total number of the FFV interaction nodes is 14,768.

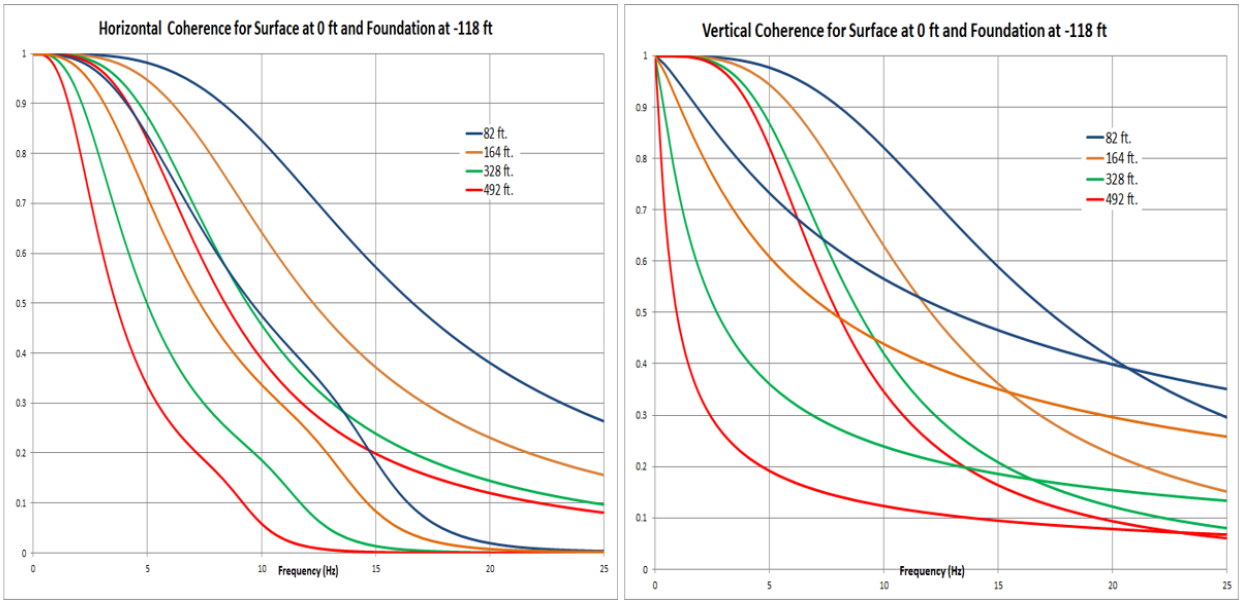


Figure 4. Horizonal (left) and Vertical (right) Coherence Functions at Surface and SMR Foundation Level

To consider the coherence variation with depth, the incoherent seismic load vector was computed for each of the 30 interaction node depth levels. At each depth level, the coherence function was obtained by interpolation between the soil coherence function at the ground surface and the rock coherence function at the SMR foundation level. To simulate the motion incoherency variation with depth, the spectral factorization of the coherence matrix was repeatedly performed for all 30 excavation depth levels. This incoherent SSI methodology is fully compliant with the US NRC DSRS SRP 3.7.2 requiremensts for SMR for considering the motion incoherency variation with depth for deeply embedded structures.

The FVROM-INT approach was applied in conjunction with the FFV interaction nodes to efficiently compute the seismic SSSI solution for coherent and incoherent input motions (Ghiocel, 2022, Hashemi et al., 2024). The FVROM-INT combines excavated soil impedance matrix condensation with the interpolation of the computed reduced excavation impedance matrix to drastically reduce the number of interaction nodes. Since the excavated soil impedance variation in frequency is much smoother than the SSI response variation, using interpolation in frequency is highly efficient for speeding up the overall SSI analysis computational effort. Only a reduced number of condensation frequencies or key frequencies, is necessary for accurately computing the condensed excavation impedance matrix and seismic load vector. Then, these are interpolated in frequency to compute them for all dense SSI frequencies.

The FVROM-INT implementation includes three computational steps described below:

1) Identify key or condensation frequencies based on free-field analysis results
2) Compute condensed excavation impedance matrix and seismic load vector for key frequencies, and interpolate excavation impedance matrix and seismic load vector for all SSI frequencies
3) Compute SSI system solutions for all frequencies using the frequency-dependent condensed excavation impedance matrix and the reduced randomized incoherent seismic reduced load vector

For the incoherent motion simulation is performed after the above Step 2 is completed, by directly randomizing the condensed seismic load vector based on the coherency matrix spectral factorization completed at each depth level (GP Technologies, 2023).

For a practical implementation of the FVROM-INT approach a reduced number of condensation frequencies of about 15-25 are usually sufficient even for highly nonuniform soils to accurately interpolate of the condensed excavated soil impedance. After the SSI response is computed, say for 180-280 SSI

frequencies, this response is further interpolated for all Fourier frequencies used for describing the input motion data in the frequency domain which may include either 8,192, 16,384 or 32,768 frequencies, or even a larger number. It should be noted that the FVROM-INT approach implementation can be used in conjunction with the "exact" FV method, but also other "approximate" methods as the different options of the FFV or ESM which are acceptable in practice. For the latter case, the solution approximations inherent to the ESM method for the full-size SSI system are transmitted to the reduced-size SSI system.

For the SSSI analysis only 22 key frequencies were sufficient for both sites. The total number of SSI frequencies was 160 for a cut-off frequency of 40 Hz for Site 1, and 240 for a cut-off frequency of 60 Hz for Site 2.

A great practical convenience is offered to structure designers and analysts by the FVROM or FVROM-INT approach since for any structured design modifications the SSI or SSSI analyses can be run extremely fast with high accuracy. Using FVROM, only the above Step 3 restart SSI analysis is required, which can be tens of times faster than using the standard SASSI analysis. This speedy computation substantially increases the efficiency of the entire SMR design process that involves iterative structure and equipment model modifications that require repeated re-analyses until the final optimized SMR design is achieved (Hashemi et al., 2024).

## COMPARATIVE CASE STUDY RESULTS

In this section comparative standalone SSI and SSSI analysis results are compared to evaluate the SSSI and motion incoherency effects.

### *Site 1 Results: Coherent Standalone SSI vs. Coherent and Incoherent SSSI*

Figures 5 through 7 show results for the deep soil site, Site 1. In these figures, the acceleration transfer function (ATF) and in-structure response spectra (ISRS) computed at the top of the SMR and the AB structures are compared.

Figures 5 and 6 show the ATF and ISRS computed at a top corner of the SMR structure from the standalone SSI and SSSI analyses. It should be noted that the SMR standalone SSI results are significantly larger. The SSSI effects drastically reduce the SMR dominant resonant ATF spectral peak at @ 3.0 Hz and produce a slight increase of the SMR response in the low frequency range, more visible in Y-direction.

The SMR incoherent ISRS are lower than the SMR coherent ISRS, except in the low frequency range Y-direction.

In contrast to SMR results, Figure 7 shows that the SSSI effects amplify the ISRS at the top of the AB structure. The SSSI effects increase the dominant ISRS spectral peak amplitude by about 50% in the X-direction (main SSSI coupling direction) that is along the AB longitudinal axis. It should be noted that in X-direction the incoherent AB response is larger increase than AB coherent response.

As shown in Figures 6 and 7, the seismic SSSI coupling effects computed for Site 1 indicate that a significant part of the vibration energy transfers from the SMR structure to the AB structure. As shown next, this energy transfer is inversed for Site 2, from the AB structure to the SMR structure.

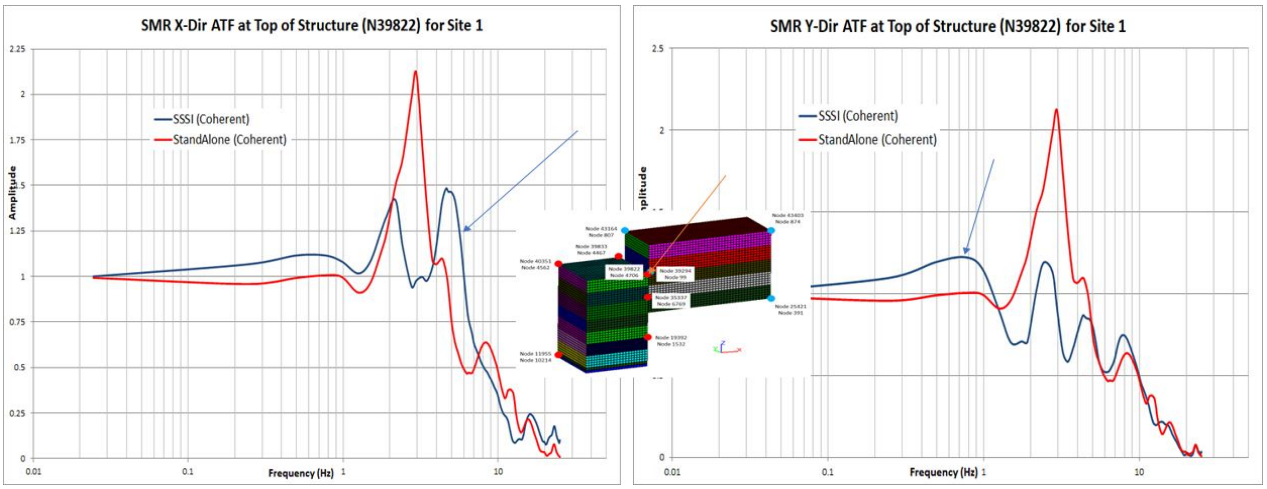


Figure 5 Standalone SSI and SSSI Coherent ATF at Top of SMR for X and Y Dir for Site 1

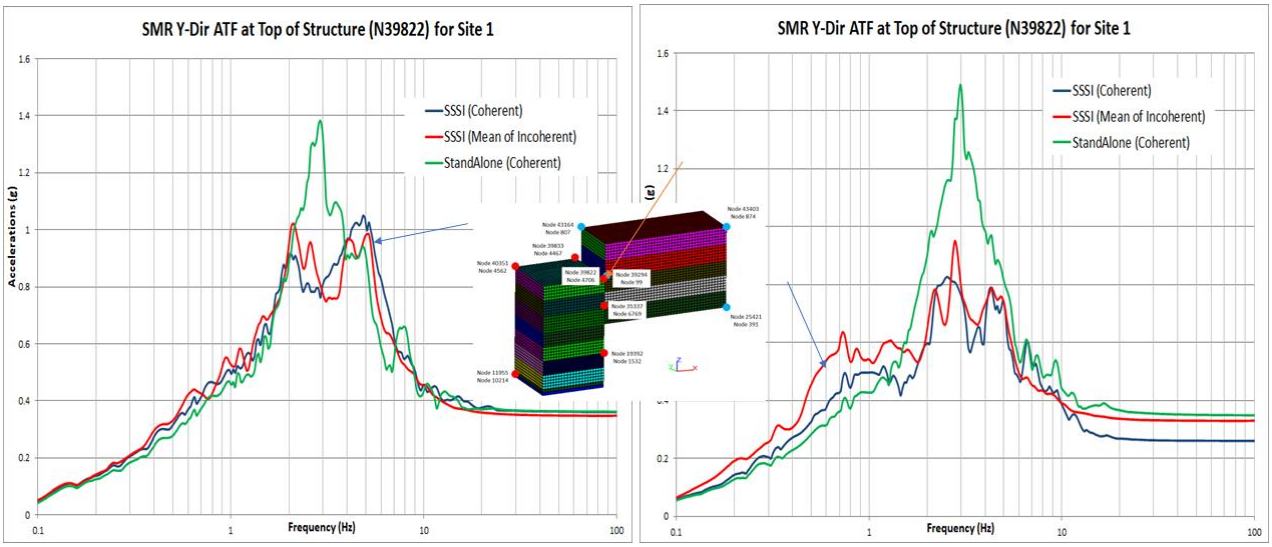


Figure 6 SSI and SSSI Coherent and Incoherent ISRS at Top of SMR for X and Y Dir for Site 1

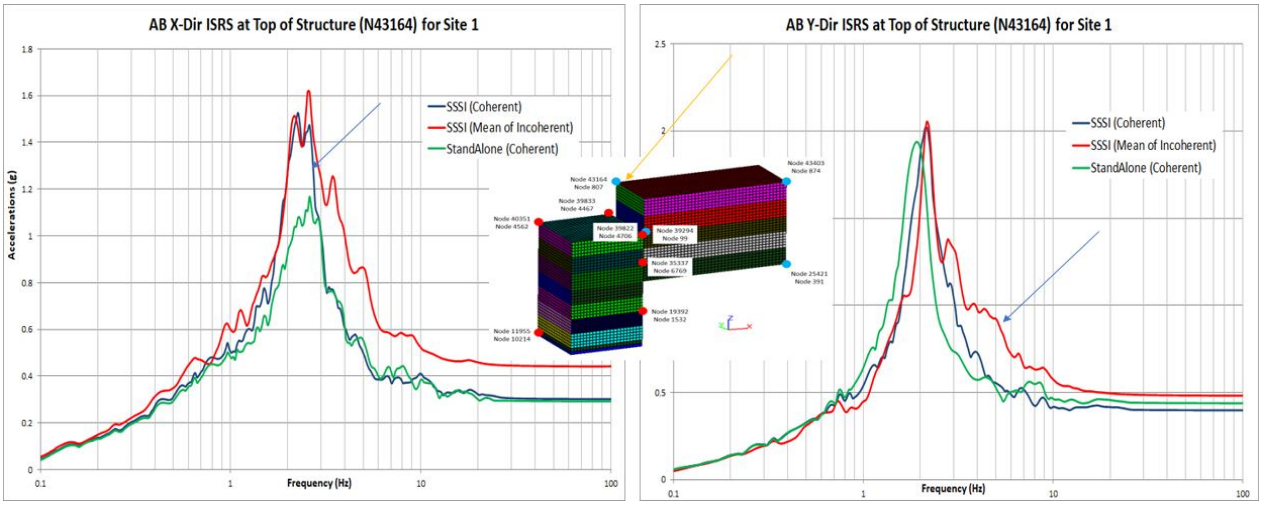


Figure 7 SSI and SSSI Coherent and Incoherent ISRS at Top of AB for X and Y Dir for Site 1

***Site 2 Results: Coherent Standalone SSI vs. Coherent SSSI***

For Site 2, SSSI effects are totally different than for Site 1. Figures 8 through 10 show the ATF computed at the top of the SMR and AB structures for the shallow soil layer site, Site 2. The SSSI effects are more complex for Site 2. The SSSI coupling effects produce for the SMR response a new dominant spectral peak @ 3.1 Hz which is close to the AB dominant spectral peak @ 2.9 Hz, while the SMR structure response is reduced in the 5-7 Hz frequency range. The increase of the SMR ATF amplitude @ 3.1 Hz is about 100%, while the decrease of in the 5-6 Hz range is about 30%.

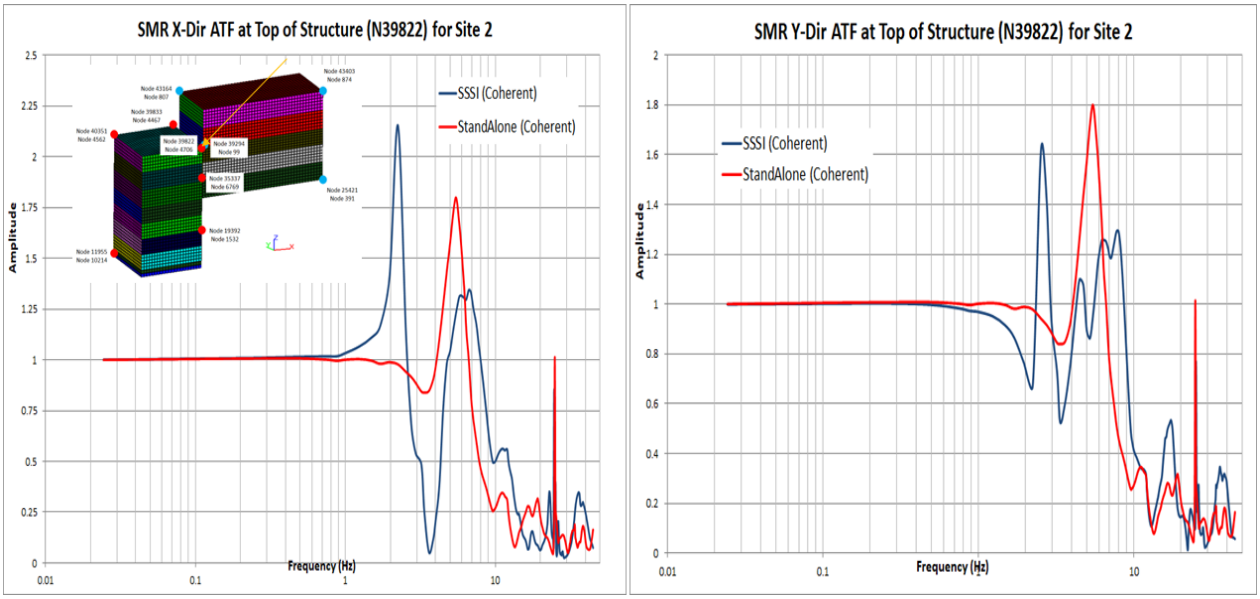


Figure 8. Standalone SSI and SSSI Coherent ATF at Top of SMR for X and Y Dir for Site 2

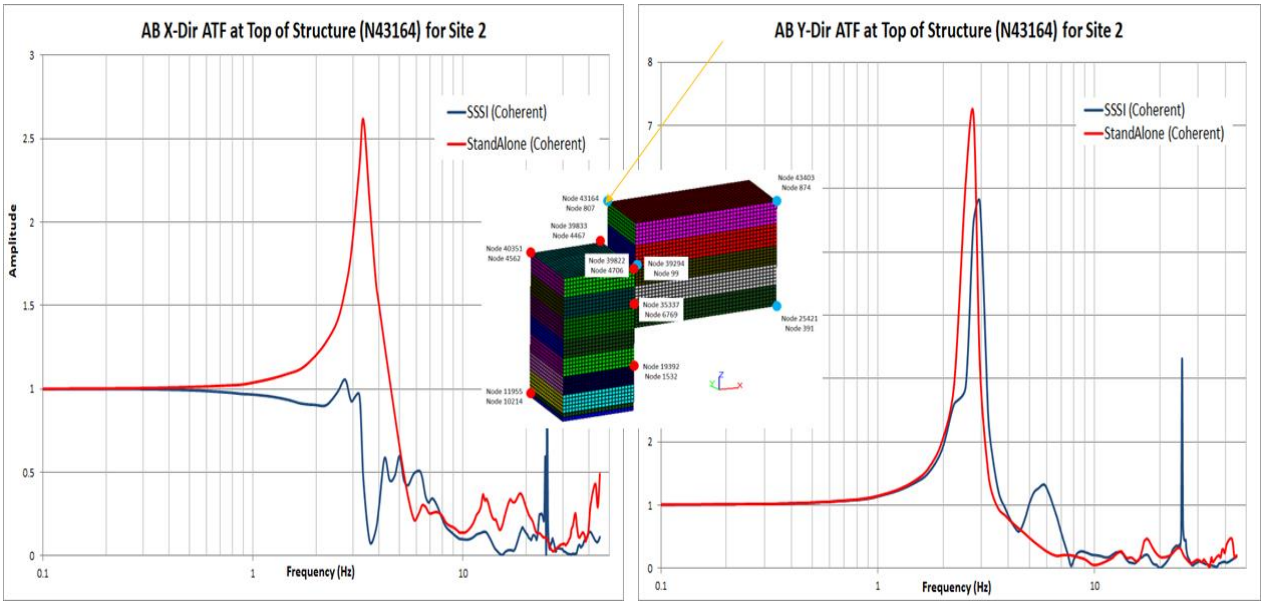


Figure 9. Standalone SSI and SSSI Coherent ATF at Top of AB for X and Y Dir for Site 2

Figure 10 summarizes the ATF results in Figure 8 and 9. It shows that due to the SSSI coupling effects, a large part of the seismic vibration energy is transferred from the AB structure to the SMR structure. This is the opposite situation with Site 1, for which a part of the seismic vibration energy was transferred from the SMR structure to the AB structure.

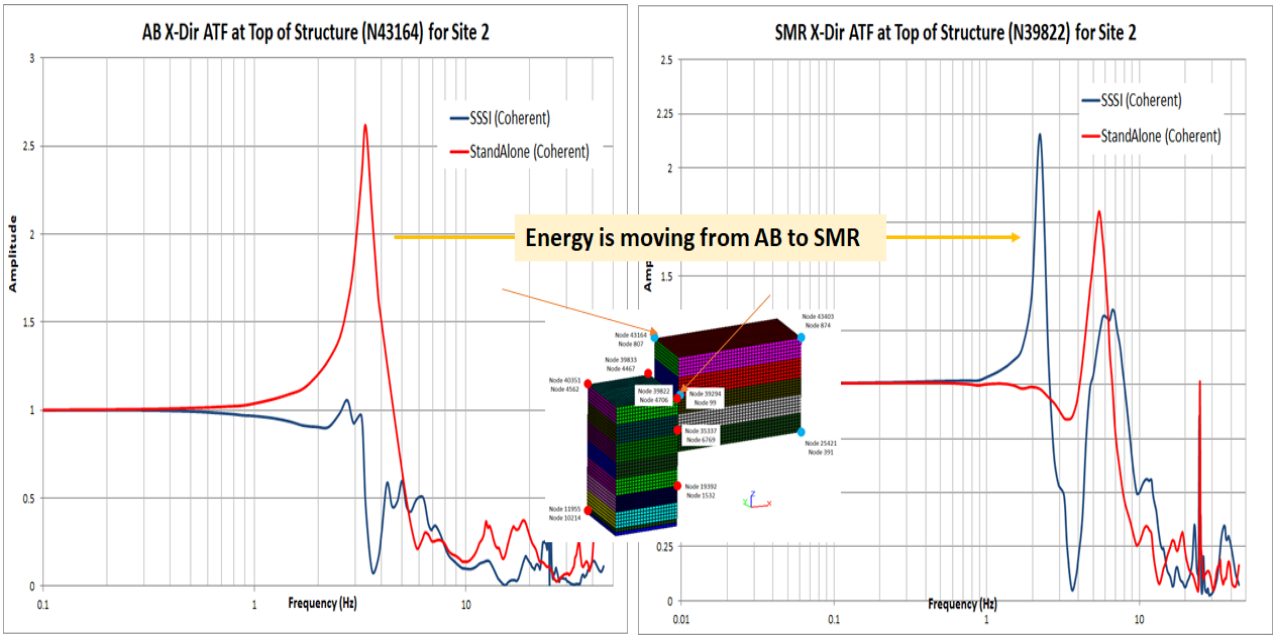


Figure 10. Standalone SSI and SSSI Coherent ATF at Top of SMR and AB for X Dir for Site 2

***Coherent and. Incoherent SSSI***

The effects of both the SSSI and the motion incoherency for Site 2 on the ISRS at the top of SMR and AB structures are illustrated in Figures 11 and 12.

From Figures 11 and 12, the SSSI effects appear to be much more significant than the motion incoherency effects. The increase of ISRS amplitude at the top of SMR structure due to the SSSI effects is about 100%, as shown in the X-direction in Figure 11. This large ISRS amplitude increase corresponds to the totally new ISRS peak at @ 2.6 Hz produced by the SSSI effects, as it was also noted for the ATF responses shown in Figure 8. Figure 12 indicates the significant decrease of the AB structure ISRS response due to thee SSSI effects.

Motion incoherency effects for both SMR and AB structures are much less than the SSSI effects.

The effects of motion incoherency variation with depth were also investigated for Site 2. The effect of the motion incoherency variation including incoherency variation with depth on the SMR structure ISRS computed at the ground surface elevation is shown in Figure 13.

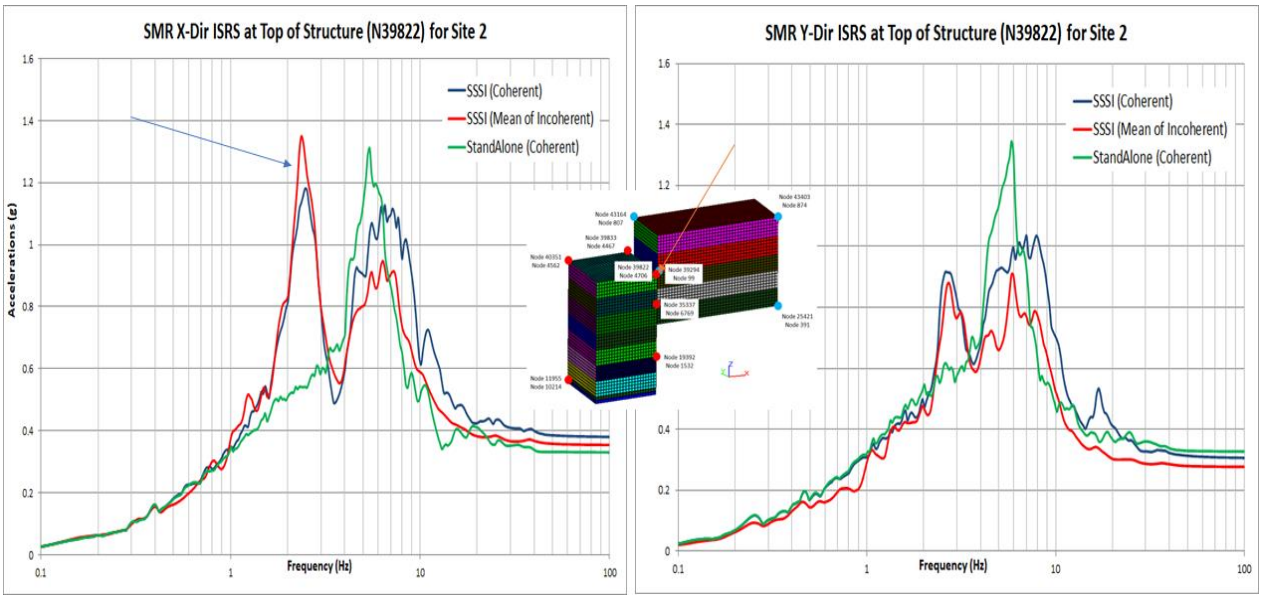


Figure 11. SSI and SSSI Coherent and Incoherent ISRS at Top of SMR for X and Y Dir for Site 2

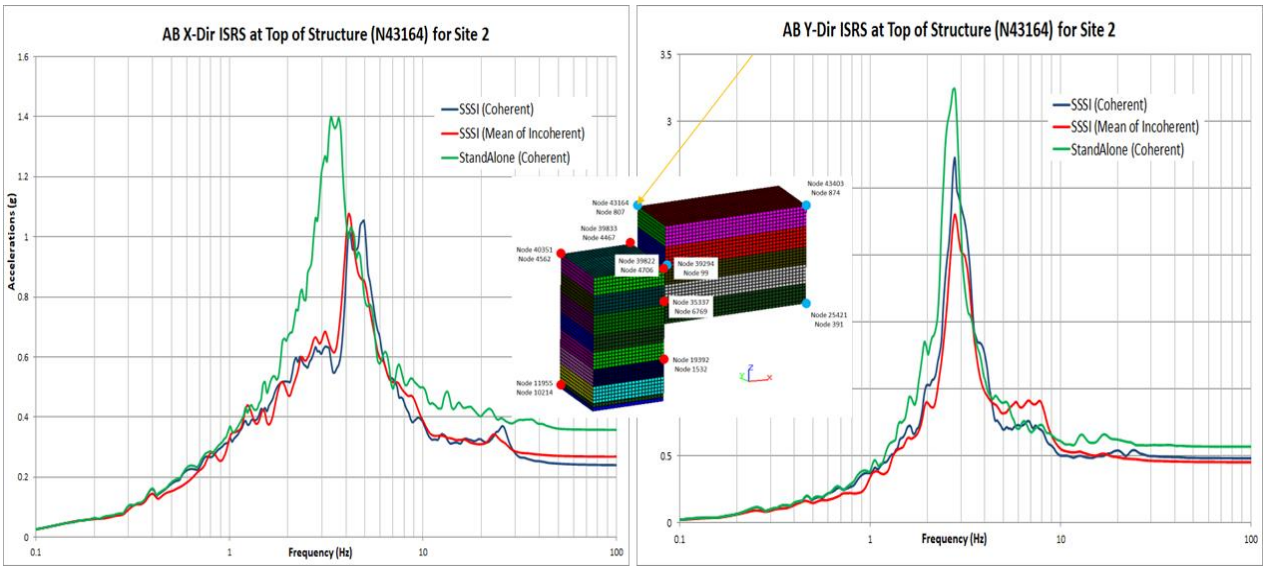


Figure 12. SSI and SSSI Coherent and Incoherent ISRS at Top of AB for X and Y Dir for Site 2

The incoherent SSSI analyses were done by assuming 1) surface coherence applied for the entire SMR embedment depth and 2) variable coherence applied for different SMR embedment levels as explained in the previous section.

Variable with depth incoherency ISRS results were only slightly higher than the constant incoherency ISRS results with 5-20 %. The largest ISRS difference of 20% noted at the ground level is shown in Figure 13. However, these differences are case-by-case dependent.

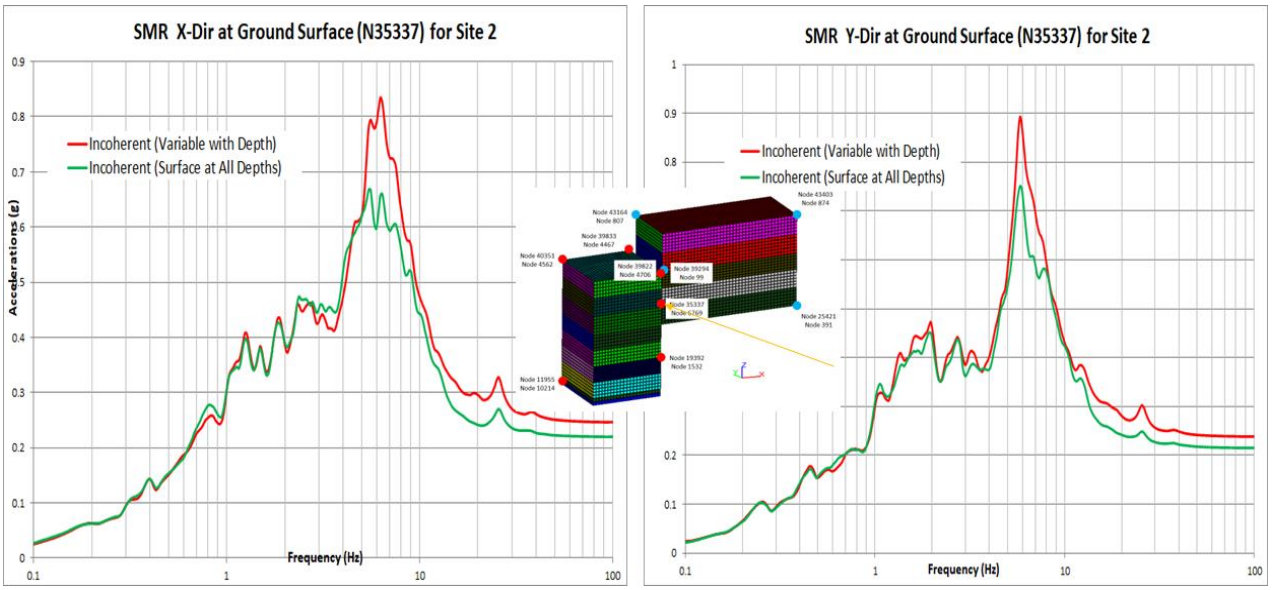


Figure 13. Comparative SMR Incoherent ISRS at Ground Level for X and Y Dir for Site 2

***Incoherent SSSI Structural Moments in SMR Wall***

The seismic forces and moments were computed in the SMR embedded wall situated at 2.5 ft near the AB structure foundation. This exterior wall is shown in Figure 14 (for X = 50 ft plane). The largest structural forces in the embedded wall were computed at a soil depth of about 25-27 ft which is close to the foundation depth of the AB structure of 26.33 ft. The motion incoherency effects amplify considerably the SSSI effects on the embedded wall in-plane forces and out-of-plane moments.

Figure 15 compares the computed coherent (red bars) and incoherent (blue bars) bending moments (MXX) in the SMR embedded wall for a horizontal slice shell elements (the X=50 ft wall plane line shown in Figure 14) at the -27.89 ft depth. Incoherent bending moments are much larger than the coherent bending moments.

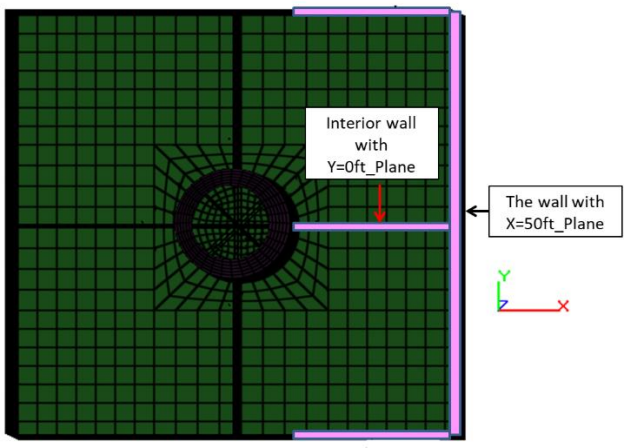


Figure 14. Selected Wall Shell Elements

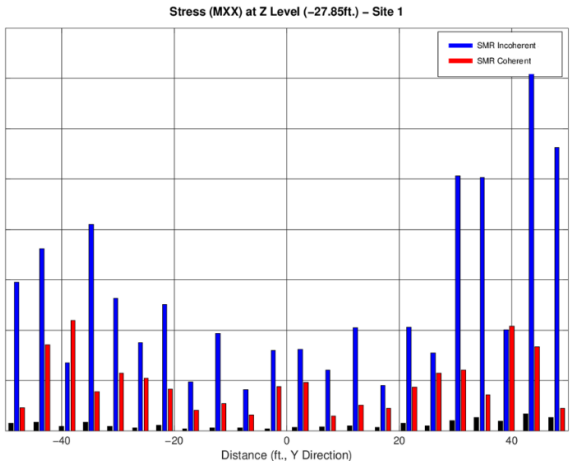


Figure 15. Comparative MXX in SMR Wall

## CONCLUDING REMARKS

The paper investigates the SSSI and the motion incoherency effects of a deeply embedded SMR structure with a nearby large AB structure.

The study results show that the *SSSI effects* were extremely important for computing the ISRS and structural forces in the embedded SMR structure. For the investigated cases, the numerical differences for SMR responses between the standalone SSI responses and SSSI responses were up to 100% or even slightly larger, for the computed ISRS and structural forces/moments in the SMR embedded wall close to AB structure.

The *motion incoherency effects* were much less significant on ISRS, but they could largely impact on the SMR embedded wall forces/moments due to the differential soil displacements impinging on the SMR walls. For the investigated cases, the motion incoherency effects increased the SMR wall forces/moments by a factor up to 2, or even more. The effects of the SMR adjacent soil nonlinear behavior, embedded wall slipping, or the wall concrete cracking which might significantly reduce these effects, were not quantified in this study so far.

Sensitivity analysis indicated that the effects of the variation of motion incoherency with depth affected only slightly the ISRS, up to 10-20%. and the SMR structural forces, up to 10-15%.

## REFERENCES

Abrahamson, N. (2007). Abrahamson, N. (2007*).”Effects of Spatial Incoherence on Seismic Ground Motions*”, Electric Power Research Institute, Palo Alto, CA and US Department of Energy, Germantown, MD, Report No. TR-1015110, December 20

GP Technologies, Inc. (2023). “*ACS SASSI NQA Version 4 User Manual, Including Advanced Options A-AA, NON, PRO, RVT-SIM and UPLIFT”*, Rev. 9, Rochester, NY, April 12.

Hashemi, A., Tarek, E., Todorovski, L, and Ghiocel, D.M. (2024). *“Site-Specific SSSI Analysis of SMR Using Flexible Volume Reduced-Order Modeling with Impedance Interpolation (FVROM-INT)”* 27th International SMiRT Conference, SMIRT27, Yokohama, March 3-8

Todorovski, L., Gomer, B, Zheng, W. and Fernandez, A. (2022). “*Geotechnical Parameters for Design of Deeply Embedded Small Modular Reactors*”, 26th International SMiRT Conference, SMIRT26, Berlin, July